Redox Biology 10 (2016) 211–220

Contents lists available at ScienceDirect

Redox Biology

journal homepage: www.elsevier.com/locate/redox

Research Paper

Oxalomalate reduces expression and secretion of vascular endothelial growth factor in the retinal pigment epithelium and inhibits angiogenesis: Implications for age-related macular degeneration

Sung Hwan Kim[a], Hyunjin Kim[a], Hyeong Jun Ku[a], Jung Hyun Park[b], Hanvit Cha[a], Seoyoon Lee[a], Jin Hyup Lee[b,c,*], Jeen-Woo Park[a,**]

[a] School of Life Sciences and Biotechnology, BK21 Plus KNU Creative BioResearch Group, College of Natural Sciences, Kyungpook National University, Daegu, Republic of Korea
[b] Department of Food and Biotechnology, Korea University, Sejong, Republic of Korea
[c] Institutes of Natural Sciences, Korea University, Sejong, Republic of Korea

ARTICLE INFO

Keywords:
VEGF
Retinal pigment epithelium
Oxalomalate
Reactive oxygen species

ABSTRACT

Clinical and experimental observations indicate a critical role for vascular endothelial growth factor (VEGF), secreted by the retinal pigment epithelium (RPE), in pathological angiogenesis and the development of choroidal neovascularization (CNV) in age-related macular degeneration (AMD). RPE-mediated VEGF expression, leading to angiogenesis, is a major signaling mechanism underlying ocular neovascular disease. Inhibiting this signaling pathway with a therapeutic molecule is a promising anti-angiogenic strategy to treat this disease with potentially fewer side effects. Oxalomalate (OMA) is a competitive inhibitor of $NADP^+$-dependent isocitrate dehydrogenase (IDH), which plays an important role in cellular signaling pathways regulated by reactive oxygen species (ROS). Here, we have investigated the inhibitory effect of OMA on the expression of VEGF, and the associated underlying mechanism of action, using *in vitro* and *in vivo* RPE cell models of AMD. We found that OMA reduced the expression and secretion of VEGF in RPE cells, and consequently inhibited CNV formation. This function of OMA was linked to its capacity to activate the pVHL-mediated HIF-1α degradation in these cells, partly *via* a ROS-dependent ATM signaling axis, through inhibition of IDH enzymes. These findings reveal a novel role for OMA in inhibiting RPE-derived VEGF expression and angiogenesis, and suggest unique therapeutic strategies for treating pathological angiogenesis and AMD development.

1. Introduction

The vascular endothelial growth factor (VEGF) family consists of a number of closely related ligands, including VEGF-A, B, C, D, E, and placental growth factor (PIGF) [1]. VEGF-A (hereafter referred to as VEGF) is a critical angiogenic factor associated with several ocular pathologies, including age-related macular degeneration (AMD) and proliferative diabetic retinopathy [2,3]. During the pathogenesis of AMD, increased VEGF expression leads to proliferation of pathological and highly permeable vessels in the subretinal space, specifically choroidal neovascularization (CNV), resulting in severe vision loss [4–6]. In adults, retinal pigment epithelium (RPE), an epithelial monolayer situated between the choroid and the photoreceptors, appears to be the only source of VEGF in the back of the eye [7,8]. Various studies demonstrated that the differentiated RPE constitutively secretes VEGF in a polarized fashion toward the basolateral side [9,10], and that its major signaling receptor, VEGFR2, is preferentially expressed by the choriocapillaris (CC) on the side facing the RPE [8,9]. VEGF-VEGFR2 binding leads to the induction of various signaling cascades including, MAPK, Akt, and Src, which is critical for the proliferation of the choroidal capillary endothelial cells and the maintenance of the fenestration of the CC [11,12]. However, upregulation of VEGF by the RPE due to age-dependent or pathological alterations is considered a critical factor in the development of CNV in AMD [13,14].

Thus, the clear involvement of VEGF in proliferative AMD has led to the development of multiple anti-VEGF drugs such as pegaptanib and ranibizumab, which are approved by the Food and Drug

* Corresponding author at: Department of Food and Biotechnology, Korea University, Sejong, Republic of Korea.
** Corresponding author.
E-mail addresses: jinhyuplee@korea.ac.kr (J.H. Lee), parkjw@knu.ac.kr (J.-W. Park).

http://dx.doi.org/10.1016/j.redox.2016.10.008
Received 12 August 2016; Received in revised form 20 October 2016; Accepted 21 October 2016
Available online 24 October 2016
2213-2317/ © 2016 Published by Elsevier B.V. This is an open access article under the CC BY-NC-ND license (http://creativecommons.org/licenses/by/4.0/).

Administration for the treatment of CNV [15–17]. All of these molecules bind to secreted soluble VEGF and prevent its interaction with VEGFR2 on the CC [18–20]. However, currently available anti-VEGF therapeutics, for the treatment of ocular neovascular diseases, do not alter retinal expression of VEGF. Consequently, current therapeutic molecules are administered repeatedly at very high doses, and systemic side effects affect their utility in the treatment of ocular disease [21,22]. Hence, therapeutic molecules designed to inhibit the underlying signaling mechanisms of retinal VEGF expression appear to have promising anti-angiogenic properties with fewer side effects.

Oxalomalate (OMA, α-hydroxy-β-oxalosuccinic acid), a tricarboxylic acid intermediate, is a well-known potent competitive inhibitor of two classes of $NADP^+$-dependent isocitrate dehydrogenase isoenzymes, which are primarily located in either the cytoplasm (IDH1) or mitochondria (IDH2) [23,24]. OMA can be formed *in vitro* and *in vivo* by condensation of oxaloacetate with glyoxylate. In fact, it is produced *in vitro* by a non-enzymatic aldol condensation between oxaloacetate and the highly reactive glyoxylate [25,26]. This reaction also occurs *in vivo* in mammalian cells under physiological conditions when oxaloacetate and glyoxylate are present, the latter being synthesized and catabolized in cells of vertebrates [27–29].

NADPH, a metabolic product of IDH enzymes, is required for the regeneration of glutathione as a reducing equivalent and thus, critical for the scavenging of cellular reactive oxygen species (ROS) by glutathione reductase and peroxidase systems [30,31]. There is a large body of research demonstrating the general effect of oxidative stress on signaling pathways, termed “oxidative interface”. During this process, ROS directly interact with critical signaling molecules including MAP kinase, PI3 kinase, Nrf-2, and ATM to initiate signaling in a variety of cellular processes, such as proliferation, metabolism, differentiation, and survival, indicating that ROS serve as critical signaling molecules [32–36].

IDH enzyme isoforms, or NADPH-generating enzymes, are major antioxidants and redox regulators that prevent oxidative stress by catalyzing the production of NADPH within different subcellular compartments [37,38]. IDH enzymes are evolutionarily conserved proteins that catalyze the oxidative decarboxylation of isocitrate to α-ketoglutarate and the reduction of $NADP^+$ to NADPH [39]. Specifically, IDH2 acts as a $NADP^+$-consuming enzyme in the forward Krebs cycle, generating NADPH for the maintenance of reduced glutathione and peroxiredoxin systems, and for self-maintenance *via* the reactivation of cysteine-inactivated IDH2 by glutaredoxin 2 [39,40].

It was recently reported that OMA contributes to the regulation of lipid metabolism by inhibiting lipid biosynthesis, linking cellular redox status, and regulating adipocyte function. Studies have indicated a decrease in IDH activity after OMA treatment, resulting in reduced plasma triglyceride and cholesterol levels and adipocyte lipoprotein lipase activity, suggesting a possible inhibitory role of OMA in fat accumulation [41]. Apart from its lipid-lowering effects, OMA has several other effects, such as enhanced apoptotic cell death in cancer cells, and an inhibitory effect on the LPS-induced inflammatory response through the induction of intracellular ROS accumulation [42–45]. However, to the best of our knowledge, there is no information available regarding the effects of OMA on CNV in AMD. Researchers have focused on the association between soluble VEGF and neovascular disease [18–20], but not on VEGF expression. Thus, in the present study, we examined the activity of OMA using *in vitro* and *in vivo* RPE cell models of AMD. The aim was determine whether OMA acts on RPE cells to modulate the expression and secretion of VEGF, thus altering the function of the retinal epithelial cells. This could represent a potential therapeutic approach to treat pathological angiogenesis and CNV development in age-related macular degeneration.

2. Materials and methods

2.1. Cell culture

RPE cells (CRL-4000) and human umbilical vein endothelial cells (Hereafter referred to as HUVECs; CRL-1730) were purchased from ATCC. The RPE cells were cultured in 37 °C, 5% CO_2 saturated humidity incubator with DMEM containing 1% penicillin-streptomycin and 10% FBS. Cells in the control group were treated as follows: the cells were cultured in the medium for 24 h, followed by culture in the medium containing 5 mM OMA (Cayman Chemical) for 24 h. Cell culture was conducted in 37 °C and 5% CO_2 saturated humidity incubator. Conditioned media (CM) from the RPE cells were established as follows: the cells were grown to 60–70% cell density in serum-free DMEM for 24 h, and the medium was then changed to the medium containing 5 mM OMA. Following culture for 24 h, the medium was replaced with new serum-free DMEM and culture was continued for 24 h. The culture supernatants were then harvested and centrifuged at 300g at 4 °C for 5 min to eliminate the intact cells after which they were concentrated and desalted by centrifugation in Amicon Ultra-15 tubes (5 kDa molecular weight cutoff; Millipore). The HUVECs were culture in a 37 °C, 5% CO_2 saturated humidity incubator with extracellular matrix (ECM) medium supplemented with 1% penicillin-streptomycin and 10% FBS. The HUVECs were cultured with CM that was collected following the exposure of the RPE cells to OMA, and the control cells were cultured in serum-free DMEM.

2.2. Cell proliferation assay

Cell proliferation was assessed by MTT assay according to the manufacturer's recommendations (Roche). Briefly, RPE cells were seeded in a 96-well culture plate with 1×10^4 cells/well, and the following day, the cells were treated as described above. Following culture for 24 h, the culture medium was removed and 100 μl MTT solution were added, followed by incubation for 4 h in an incubator at 37 °C; the MTT solution was then removed and 100 μl DMSO were added to each well, followed by mixing for 10 min, and the OD value was then measured at 540nm using a Ultrospec 2100-pro spectrophotometer (Amersham Biosciences). Proliferation of HUVECs was assessed as follows: the cells were treated as described above. Then, the cells were washed with PBS twice, fixed for 20 min in 3:1 methanol: acetic acid, rinsed with water, stained with 5% crystal violet or 1 μg/mL propidium iodide, and counted. Cell proliferation was calculated from the ratio of the number of cells in the treated samples to those in the control plates.

2.2.1. In vitro cell migration assay

In vitro, the scratch-wound assay was used to detect the migration of HUVECs, as described previously [46]. HUVECs were grown to 80–90% confluence in 12-well plates in serum-free DMEM. Plates were mechanically scratched with a sterile 10 μl pipette tip to create two perpendicular linear scrapes. The cells were extensively rinsed with phosphate-buffered saline (PBS) to remove cellular debris before treating with CM in the serum-deprived condition to determine the contribution of cell proliferation to the wound healing. The progression of migration was photographed immediately and 24 h after wounding in the same field, near the crossing point, using digital camera (Nikon) connected to a Zeiss Axiovert 200 inverted microscope. Extent of wound healing was determined by the distance traversed by cells migrating into the denuded area. The horizontal lines indicate the wound edge. Migration of HUVECs across the wound margins from 24 h was assessed and photographed by inverted microscopy. Original wound area width- Wound area width of 24 h after injury=Recovered area width (% of the control recovered are width). Recovered area width is means that HUVEC cell migration distance or Wound closure rate is (Wound $area_{0\ h}$–Wound $area_{24\ h}$)×100/Wound $area_{0\ h}$.

Representative data is cumulative of three independent experiments.

2.2.2. In vitro angiogenesis assay

The cells were plated with Matrigel (BD Biosciences), and the HUVECs were stimulated to form capillary tube-like structure, as previously described [47]. Matrigel (60 μl) was added to a well of a 96-well plate, and the culture plate was shaken gently. Following Matrigel solidification, a 100 μl suspension of HUVECs was added to each well at a cell density of 1×10^4. The cells were then treated with CM, and cultured in a 37 °C, 5% CO_2 incubator for 24 h. For fluorescent monitoring of tube formation, prior to harvesting, HUVECs were incubated for 30 min with 2 μM Calcein AM (BD Biosciences) at 37 °C. The cells were harvested and counted, and a single cell suspension at 1×10^6 cells/mL was prepared. The cells were diluted in serum-free DMDM in the presence of CM. The cells were added at a density of 1×10^4 per 100 μl to each well and incubated for 24 h in a CO_2 incubator at 37 °C. The tube formation was visualized directly through a Zeiss Axiovert 200 inverted microscope, and phase contrast photomicrographs were acquired. Wherever Calcein AM was used during assay, tube formation was visualized by using a Zeiss fluorescence Axiovert 40 CFL inverted microscope (485 nm excitation/520 nm emission). To analyze angiogenic activity after treatment with respective substances, the extent of tube formation in each cell population was quantified by measuring the cumulative tube length with ImageQuant 5.2 software (Molecular Dynamics).

2.3. ELISA assay

Secreted VEGF concentrations were measured using commercially available enzyme-linked immunosorbent assay (ELISA) kits according to the manufacturer's instructions (R & D Systems). Volumes of CM were normalized to the total number of cells present at the time of collection.

2.4. RT-PCR

Total RNA was extracted from cultured cell using an RNeasy Mini Kit according to the manufacturer's instructions (Qiagen). Purity of the RNA samples was assessed by determination of the optical density at 260:280 nm. Three micrograms of total RNA was used for cDNA synthesis using GoScript Reverse Transcription System (Promega). Sequences of the primers used were as follows: for HIF-1α, 5′ CAACCCAGACATATCCACCTC and 3′ CTCTGATCATCTG-ACCAAAAACTCA; for VEGF, 5′ GCTTGTCACATCTGCATTCAC and 3′ AGTCCAACATCACCATGCAG; for Actin, 5′ AAGTCAGTGT-ACAGGTAAGCC and 3′ GTCCCCCAACTTGAGATGTATG. All reactions were performed for 30 cycles with the following temperature profiles: 95 °C for 3 min (initiation; 30 s/cycle thereafter); 55 °C for 45 s (annealing); and 72 °C for 45 s (extension). 10 μl of PCR products was then separated on 2% agarose gels and bands were visualized with ethidium bromide staining. Quantification of PCR products was performed with ImageQuant 5.2 software.

2.5. Immunoblot analysis

The Following commercial antibodies and reagents were used: VEGF, HIF-1α, pVHL, phospho-Chk2, phospho-ATM, and Ubiquitin (Cell Signaling Technology); phospho-E2F1 and Prx-SO_3 (Abcam); Prx-SO_3 (AbFrontier); IDH1 and IDH2 (Sigma Aldrich); and Actin (Santa Cruz Biotechnology). Conventional immunoblotting procedures were used to detect the target proteins: cells were collected, washed once in cold PBS, and then scraped in TEGN buffer (10 mM Tris, pH 8, 1 mM EDTA, 10% glycerol, 0.5% Nonidet P-40, 400 mM NaCl, 1 mM DTT, 0.5 mM phenylmethylsulfonylfluoride, and protease inhibitor mixture containing 1 M benzamidine, 3 mg/mL leupeptin, 100 mg/mL bacitracin, and 1 mg/mL α2 macroglobulin) and incubated on ice for 15 min. Lysates were then cleared by centrifugation at 20,000 *g* for 10 min. Total protein concentration was determined *via* the Bio-Rad protein assay. Equal amounts of protein were separated on 10% SDS-PAGE and the proteins were transferred to nitrocellulose membranes (Bio-Rad). The membranes were then blocked for 1 h in a PBS solution containing 5% nonfat milk powder and 0.1% Tween-20 and then probed with primary antibody overnight in 1% milk, 0.1% Tween-20 in PBS. After washing, membranes were incubated for 1 h with horseradish peroxidase-linked secondary antibody (Sigma Aldrich) in 1% milk, 0.1% Tween-20 in PBS. Finally, after three 5-min washes in 0.1% PBS/Tween-20, proteins were visualized by enhanced chemiluminescence (Amersham Biosciences). Band intensities were quantified with ImageQuant 5.2 software.

2.6. Immunocytochemical analysis

To study the expression of VEGF, immunofluorescence staining of VEGF was performed on RPE cells. Cells were grown on coverslips for 24 h. Thereafter, cells were treated with OMA as indicated. Cells were washed with PBS and fixed with 4% paraformaldehyde, permeabilized with 0.5% Triton X-100 in PBS, and pre-treated with blocking solution. After fixation and after blocking the non-specific binding, the coverslips were incubated with antibodies against VEGF (Cell Signaling Technology) at 4 °C overnight, followed by the incubation with FITC-conjugated secondary antibodies (Vector Laboratories) for 1 h at room temperature in the dark. After washing, cells were counterstained with DAPI and the coverslips were mounted on DakoCytomation Fluorescent Mounting Medium (DAKO). The preparations were analyzed with the inverted fluorescence microscope. Image analysis was performed using the ImageQuant 5.2 software.

2.7. Proteasome inhibition and immunoprecipitation

RPE cells were treated with 20 μM of MG-132 (Sigma Aldrich) in the presence of absence of OMA as indicated and then protein stability was assayed by conventional immunoblotting. For ubiquitination assay, the RPE cells were washed with ice-cold PBS and lysed in buffer containing 150 mM NaCl, 50 mM Tris–HCl, pH 7.4, 1% NP-40, 1 mM NaF, 1 mM Na_3VO_4, and EDTA-Free Halt Protease Inhibitor Cocktail (Thermo Scientific Pierce) for 30 min on ice. Total cell lysates (1 mg of protein) were subjected to immunoprecipitation with 2 μg of anti-HIF-1α for 1 h at 4 °C. Protein G Sepharose (GE Healthcare Bio-Sciences AB) was added and incubation continued overnight at 4 °C. Immunoprecipitated cell lysates were subjected to 10% SDS-PAGE, and ubiquitinylated HIF-1α was detected with anti-ubiquitin antibody (Santa Cruz Biotechnology). ImageQuant 5.2 was used for quantifying the protein levels based on band density exhibited in the immunoblot photographs.

2.8. Measurement of redox status and cellular ROS

The concentration of total glutathione was determined by the rate of formation of 5-thio-2-nitrobenzoic acid at 412 nm ($\varepsilon=1.36\times10^4$ M $M^{-1}cm^{-1}$) according to the method described by Akerboom and Sies [48]. Oxidized glutathione (GSSG) was measured by the 5,5′-dithiobis(2-nitrobenzoic acid)-GSSG reductase recycling assay after treating GSH with 2-vinylpryidine [49]. NADPH was measured using the enzymatic cycling method as described previously [50] and expressed as the ratio of NADPH to the total NADP pool. Intracellular ATP levels were determined by using luciferin-luciferase, as previously described [51]. Light emission was quantitated in a Turner Designs TD 20/20 luminometer (Stratec Biomedical Systems). Intracellular ROS production and mitochondrial membrane potential was measured using the oxidant-sensitive fluorescent probe DCFH-DA and cationic reagent JC-1 (Molecular Probes), respectively, with FACS analysis (BD Biosciences) [52]. Fluorescence intensity was expressed in

arbitrary units on a logarithmic scale. Mitochondrial ROS formation was visualized as follows: MitoSOX (Invitrogen) was added at 5 μM in the medium and after incubation for 10 min, cells were fixed with 4% paraformaldehyde for 10 min, mounted onto glass slides with Mowiol, and observed under the fluorescence inverted microscope. Quantitation was performed by selecting the cellular region of 20–30 cells for each sample and measuring the intensity of the MitoSOX fluorescence using ImageQuant 5.2 software.

2.9. Mouse xenograft model

RPE cells or HUVECs at subconfluence were harvested, washed with PBS, and resuspended in the serum-free medium. A total 1.5×10^6 cells were mixed with an equal volume of the Matrigel in the presence or absence of the respective substances. The mixture was immediately inoculated s.c. into both flanks of 6-week-old male athymic nu/nu mice. The animals were bred and kept under defined-flora pathogen-free conditions at the Animal Facility of the University Laboratory Animal Resources, Kyungpook National University. All experiments were performed in accordance with the guidelines of the University Institutional Animal Care and Use Committee. The animals were monitored for Matrigel plug size at 2-d intervals throughout the period of the study. The animals were sacrificed 14 days after the implantation and the Matrigel plugs were carefully excised without other adjacent tissues. The excised plugs were photographed immediately and the specimens were subjected to immunohistochemistry analysis described below.

2.10. Histological analysis

Specimens of Matrigel plugs were fixed in 4% (w/v) paraformaldehyde in PBS, and processed by conventional paraffiin-embedded method. The paraffin-embedded tissue sections with thickness of 5 μm were heat-immobilized, deparaffinized using xylene, then rehydrated in a series of increasing ethanol concentrations. Antigen retrieval was performed by incubating the sections in 10 mM sodium citrate (pH 6.0) and heated to 90 °C for 20 min. Immunohistochemistry was performed using a VECTASTAIN ABC Kit (Vector Laboratories), according to the manufacturer's instructions, using antibody against PECAM, VWF, and ERG (Santa Cruz Biotechnology), phospho-E2F1 (Abcam), and pVHL, HIF-1α, VEGF, phospho-Chk2, and phospho-ATM (Cell Signaling Technology). Histological studies of mouse eyes were performed according to previously published protocols [53]. Eyes from each group were enucleated, fixed in 4% paraformaldehyde, and embedded in a composite paraffin block. Then, the 5-μm-thick tissue sections were deparaffinized, rehydrated, and used for hematoxylin and eosin staining and immunofluorescence. Antibody used to identify the RPE cells was anti-cytokeratin 18 (Santa Cruz Biotechnology). The sections were counterstained with DAPI (Vector Laboratories). Images were acquired with a Zeiss Axiovert 200 inverted microscope or a Zeiss LSM 510 laser scanning confocal microscope. Staining intensities were analyzed using color deconvolution feature of ImageQuant 5.2 software (Molecular Dynamics).

2.11. CNV induction and therapeutic intervention

8-week-old male C57BL/6 J mice were used in this study. The animals were housed in climate-controlled, specific pathogen-free barrier facilities under a 12-h light-dark cycle, and chow and water were provided *ad libitum*. The Institutional Animal Care and Use Committee at the Kyungpook National University approved the experimental protocols for this study. CNV was induced by subretinal injection of PEG in accordance with the protocols as previously documented [54,55]. In brief, the eye of animals was decompressed with a 27-gauge needle by inserting the needle through the conjunctiva and sclera 1 mm behind the limbus. A UMP3 Microinjector equipped with a Nanofil 100 μl syringe and 33-gauge blunt needle (Word Precision Instruments) was used for injections. Needle movement was stopped when light resistance was felt by the operator. Subsequently, a single injection of 0.5 mg of PEG-8 (PEG with a mean M_r of 400; Spectrum Chemical) dissolved in 2 μl of sterile PBS was then administered in 10 s. Formation of a subretinal bleb was controlled through observation using the microscope. Local administration of OMA was performed by intravitreal injection, immediately following the induction of CNV [56]. In brief, the eye was proptosed and held in position with a pair of forceps, while 4 μg of OMA/4 μl of PBS was injected using a 33-gauge hypodermic needle (Sigma Aldrich). The injection site was treated with chloramphenicol and globe reposited. The eyes were enucleated at day 3 post-injection, and subjected to retina and RPE/choroid tissue processing for the histological analysis.

2.12. Statistical analysis

Results are shown as means ± SD, which were performed using a two-tailed *t*-test.

3. Results and discussion

3.1. Effect of OMA on VEGF expression and angiogenesis

To determine whether OMA can directly inhibit VEGF expression in RPE cells, we treated these cells with OMA (5 mM) for 24 h; CM were collected and the level of VEGF was measured by ELISA. VEGF levels were normalized to cell numbers and those of medium volume. As shown in Fig. 1A, OMA treatment led to a decrease in VEGF production in RPE cells in comparison to that in control cells. Furthermore, in agreement with the data in Fig. 1A, we also found a significant reduction of VEGF protein in RPE cells treated with OMA, compared to that in control cells (Fig. 1B and C), indicating that OMA treatment clearly reduces VEGF expression and secretion. To determine if reduced VEGF expression occurred at the mRNA level, RT-PCR was used to assess VEGF mRNA expression. As shown in Fig. 1D, we observed a significant reduction in VEGF mRNA in OMA-treated RPE cells compared to that in control cells, indicating that OMA could inhibit VEGF transcription. To exclude the possibility that the decrease in VEGF production was due to inhibition of cell proliferation, we analyzed cell proliferation using an MTT assay, under the same experimental conditions. OMA treatment had little effect on the proliferation of RPE cells, when compared to that of control cells (data not shown). These results suggest that the inhibition of VEGF production by OMA was not through modulation of cell proliferation or death. Collectively, these results suggest that OMA reduces VEGF production through inhibition of expression at the transcriptional level.

Angiogenesis involves multiple events in endothelial cells, including cell proliferation, migration, and tube formation, and VEGF plays a central role in these processes. Endothelial cells respond to VEGF with mitogenesis, followed by the organization of cells into new vessels [57,58]. To determine the anti-angiogenic potential of OMA, and its potential mechanism of action through VEGF inhibition, *in vitro* angiogenesis assays measuring proliferation, transmigration, and tube formation were performed in HUVECs. RPE cells were cultured with or without OMA (5 mM) for 24 h, and CM were applied to HUVECs in a series of angiogenic assays.

Initial experiments were performed to evaluate endothelial proliferation by counting total number of HUVECs after crystal violet staining. We found that proliferation increased after stimulation with CM derived from RPE cells, but was significantly inhibited when HUVECs were cultured in CM prepared from OMA-treated RPE cells (Fig. 1E). To further assess OMA's anti-angiogenic activity, which was suggested by the downregulation of VEGF, motility and tube formation assays were performed using HUVECs. As shown in Fig. 1F and G,

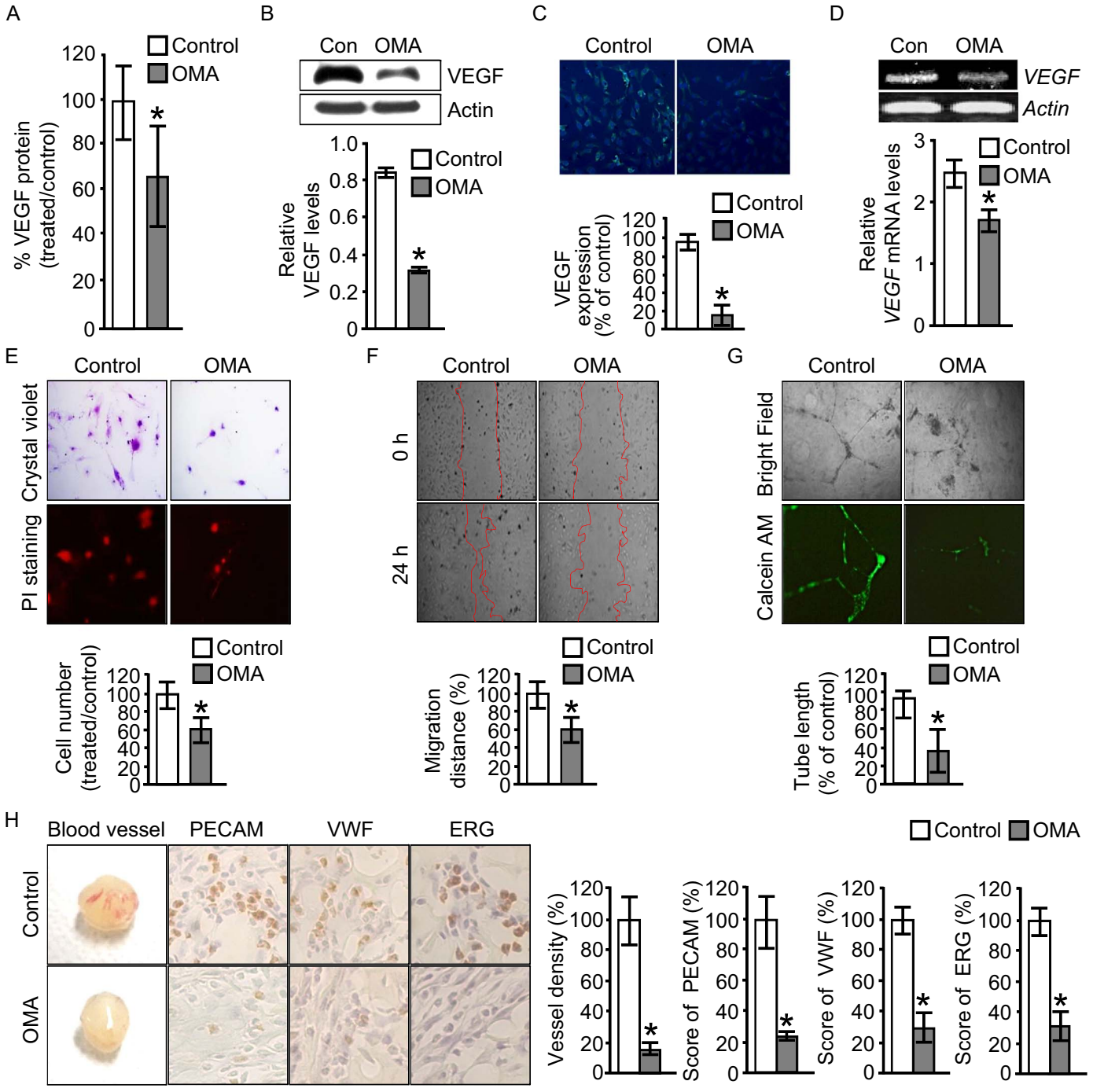

Fig. 1. OMA inhibits VEGF expression and angiogenesis. (A) The levels of VEGF in CM of RPE cells. The data were expressed as a percentage of control treated with PBS. (B) Immunoblot analysis of intracellular expression of VEGF in the RPE cells. Actin was used as a loading control. Quantifications of the levels of VEGF normalized to actin are shown. (C) Representative images of immunofluorescence staining of VEGF in the RPE cells. Histograms represent the quantification of fluorescence intensity. Nuclei were counterstained with DAPI. (D) RT-PCR analysis of mRNA levels of VEGF in the RPE cells. *Actin* was used as an internal control for the experiment. The mRNA levels were normalized to the actin level. (E) Cell proliferation assay for HUVECs incubated with CM for 24 h. Cells were then stained with 5% crystal violet or propidium iodide (PI) and scored. Data are represented as a ratio to control treated with CM prepared from PBS-treated RPE cells. (F) Representative images of migration of HUVECs cultured for 24 h in the presence of CM. Extent of the cell migration distance was calculated as described in Materials and Methods. Changes in the extent of the transmigration distance were represented as a percentage of the control group. (G) Morphological appearance and capillary tube formation of HUVECs in the presence of CM grown on Matrigel for 24 h as shown in bright field and fluorescence micrograph of Calcein AM-stained HUVECs, respectively. Quantitative image analysis depicting the total tube length of angiogenic structure as a percentage of control. (H) Macroscopic appearance of neovascularization and immunohistochemical staining of angiogenesis markers in Matrigel plugs from HUVECs treated with CM. Quantitative results of blood vessel density and expression levels of the angiogenic markers are shown as a percent of control. Each value represents the mean ± SD from three independent experiments. *$P < 0.01$, *versus* control group. The figure shows representative data for three independent experiments.

OMA inhibited migration and tube formation in HUVECs induced by CM prepared from RPE cells. The effects of OMA on angiogenesis-associated endothelial cell functions observed *in vitro* were confirmed *in vivo* in the Matrigel angiogenesis assay. Immunodeficient mice were subcutaneously injected with Matrigel suspensions containing HUVECs treated with CM derived from either untreated or OMA-treated RPE cells. As seen in Fig. 1H, neovascularization was observed in HUVECs stimulated with CM from untreated RPE cells. However,

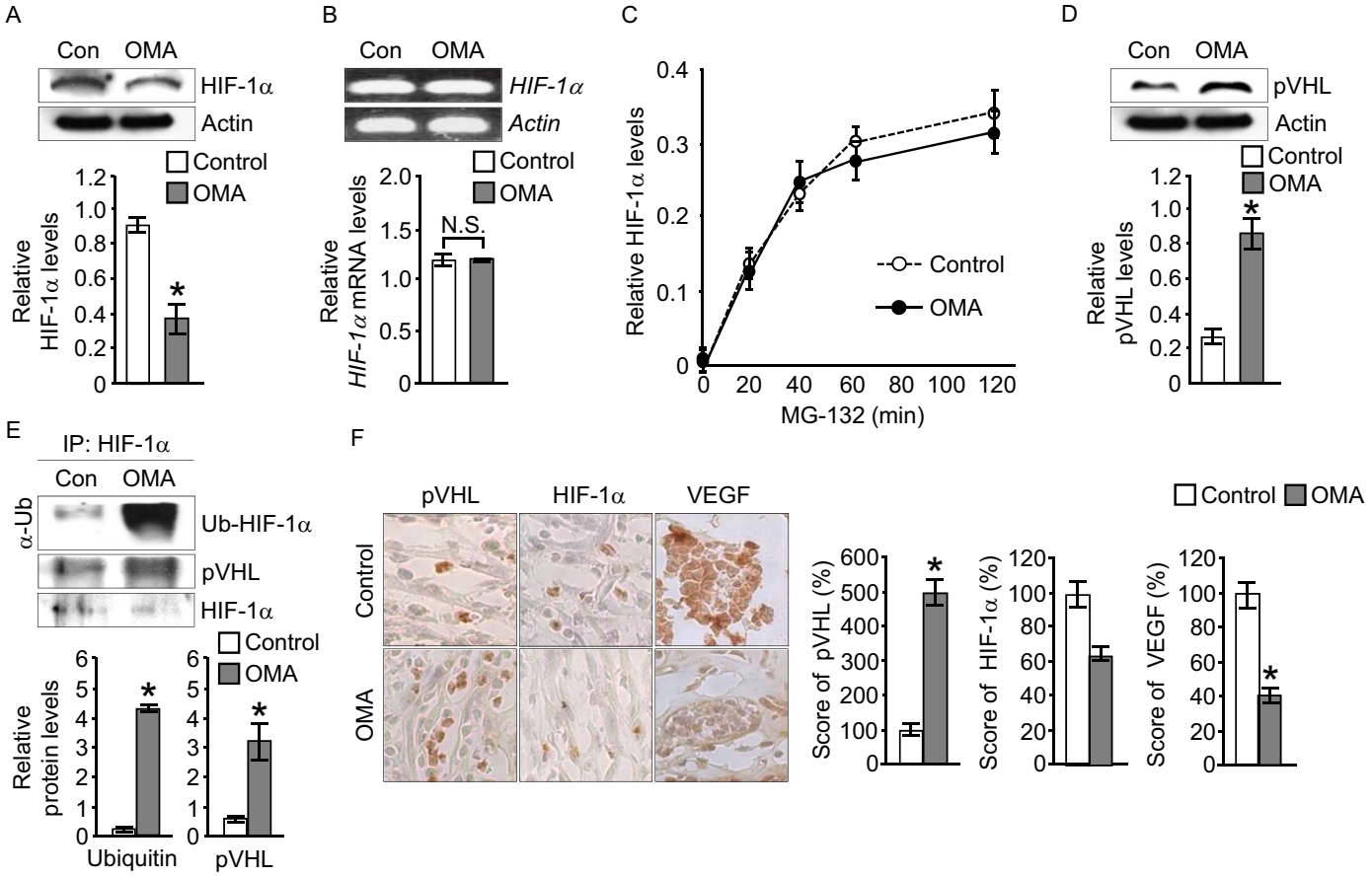

Fig. 2. OMA promotes degradation of HIF-1α by pVHL-mediated ubiquitination. (A) Immunoblot analysis of HIF-1α levels in the RPE cells after OMA treatment. Actin served as a loading control. The proteins levels were normalized to the actin level. (B) Quantitative RT-PCR analysis of mRNA expression of HIF-1α gene in the RPE cells. *Actin* was examined as a loading control, and a graph depicting the quantification of the relative abundance of the gene is shown. N.S. indicates no significant difference compared to control. (C) Decay kinetics of HIF-1α. For immunoblots of HIF-1α, the RPE cells were treated with 20 μM of MG-132 in the presence or absence of OMA for the indicated times. Immunoblot of total actin was included as a loading control. Relative levels of the HIF-1α protein in the immunoblot were determined by measuring the density of the HIF-1α protein band and normalized to that of actin. The data are expressed as a ratio to control at time zero. (D) pVHL is highly induced in the RPE cells by OMA treatment. The cells were treated with 5 mM OMA and harvested 24 post-treatment, and pVHL induction was probed by immunoblotting, using actin as a loading control. Results of pVHL quantification are normalized to the expression of actin and shown. (E) OMA increases ubiquitination of HIF-1α by upregulation of pVHL activity. The RPE cell lysates were immunoprecipitated with anti-HIF-1α antibody, and immunoblotted with anti-pVHL and anti-ubiquitin antibodies. Immunoblot of total HIF-1α is included as a loading control. Relative band intensities normalized to HIF-1α are shown. (F) Immunohistochemical staining for protein expression of VEGF and pVHL-mediated HIF-1α degradation on Matrigel plugs mixed with the PRE cells in the presence of 5 mM OMA. Nuclei are stained with Harris hematoxylin. Quantitative results of the expression levels of the indicated proteins are represented as a percentage of control. The figure shows representative data for three independent experiments. Error bars represent mean ± SD (n =3). *$P < 0.01$, *versus* control group.

this effect was prevented when HUVECs were treated with CM derived from OMA-treated RPE cells. Taken together, these results suggest that OMA possesses potent anti-angiogenic activity.

3.2. Effect of OMA on HIF-1α protein expression

To explore the possible mechanism of VEGF inhibition by OMA, we determined whether OMA could modulate the levels of HIF-1α, a major regulator of VEGF expression. The regulation of VEGF is mediated primarily through the transcription factor HIF-1α [3]. We treated RPE cells with OMA and then examined the effect on HIF-1α protein levels. As shown in Fig. 2A, we found that HIF-1α expression in RPE cells was suppressed by OMA treatment. To address whether HIF-1α is involved in the regulation of VEGF expression in the RPE cells, we performed RNA interference of HIF-1α using siRNA; VEGF expression was significantly reduced in cells transfected with siRNA against HIF-1α but not in the cells transfected with control siRNA (data not shown).

We next asked whether inhibition of HIF-1α protein accumulation by OMA could be a result in transcriptional inhibition. However, RT-PCR showed no significant changes in HIF-1α mRNA levels in RPE cells after OMA treatment (Fig. 2B). These results suggest that OMA suppresses HIF-1α protein accumulation probably through a post-transcriptional mechanism. One possible post-transcriptional mechanism for the inhibitory activity of OMA is increased degradation and/or reduced synthesis of HIF-1α protein. To determine the point at which OMA interferes with inhibition of HIF-1α protein expression, we examined the accumulation of HIF-1α in RPE cells after treatment with a proteasome inhibitor, MG-132, to prevent HIF-1α degradation. HIF-1α rapidly accumulated over a period of 2 h in the presence of MG-132. Of particular interest, the accumulation rates of HIF-1α in the presence or absence of OMA appeared comparable (Fig. 2C), strongly suggesting that the inhibitory effect of OMA on VEGF and HIF-1α protein expression is mediated primarily through directly promoting HIF-1α degradation, not by suppressing the synthesis of HIF-1α.

Next, we wished to understand how HIF-1α protein degradation is promoted in the presence of OMA. It is well established that the pVHL tumor suppressor plays a critical role in the regulation of HIF-1α stability, *via* ubiquitination and proteosomal degradation through E3 ubiquitin ligase activity [59,60]. In addition, pVHL mutations prevent its interaction with HIF-1α, which accumulates and stimulates the expression of several genes encoding growth factors such as VEGF that are responsible for neovascularization [61,62]. Hence, pVHL is an important tumor suppressor that inhibits the growth of angiogenic tumors, mainly by depressing HIF-1α-mediated VEGF expression in

response to DNA damage or oxidative stress [60]. To examine the contribution of OMA to pVHL activity and subsequent pVHL-mediated ubiquitination of HIF-1α, we treated RPE cells with OMA and analyzed the expression of pVHL (Fig. 2D) and the ubiquitination of HIF-1α (Fig. 2E). The data revealed that OMA treatment induced upregulation of pVHL (Fig. 2D), and importantly, increased pVHL activity was reflected on the stimulation of HIF-1α ubiquitination (Fig. 2E), suggesting that OMA promotes the degradation of HIF-1α through pVHL-mediated ubiquitination.

As a further proof that OMA could inhibit VEGF expression by targeting HIF-1α to pVHL-mediated destruction, Matrigel mixtures with RPE cells in the presence or absence of OMA were subcutaneously injected into the flank region of immunodeficient mice. Following this treatment regimen, the Matrigel plugs were harvested and processed through immunohistochemical staining with the indicated antibodies. Fig. 2F shows that administration of OMA drastically inhibited the expression of VEGF *via* activation of pVHL-mediated HIF-1α degradation compared to that in the control samples, which is in agreement with data presented in Fig. 2E. This provides a mechanistic explanation for the response of the retinal pigment epithelium to OMA. Thus, these results support the conclusion that OMA suppresses VEGF expression by intervening with pVHL-mediated activation of HIF-1α degradation.

3.3. Effect of OMA on the E2F1 pathway

The data presented so far indicate that OMA upregulates pVHL activity in the RPE cells, which is associated with inhibition of VEGF production through HIF-1α degradation. However, this data did not provide insight into the nature of this association. We considered the E2F1 transcription factor as a potential candidate to establish a link between pVHL activity and OMA because pVHL is a direct downstream target of E2F1 [63]. In addition, recently it was reported that the phosphorylated and active form of E2F1 is regulated in ROS-dependent manner [64,65]. ROS-dependent phosphorylation of E2F1 has previously been investigated in some detail. ATM protein kinase is phosphorylated by cellular ROS to act as a redox sensor in cells, and ROS-dependent phosphorylation of ATM activates the effector kinase Chk2, which in turn phosphorylates its downstream target, E2F1 [32,64,66,67].

Hence, to address whether regulation of pVHL activity is mediated by phosphorylation and activation of the ATM-Chk2-E2F1 axis, we tested the effect of OMA on the phosphorylation of components involved in this signaling pathway. As apparent in Fig. 3A, we found that OMA could activate the phosphorylation of E2F1, Chk2 kinase, and E2F1 transcription factor. Moreover, in accordance with the data in Fig. 3A, in the Matrigel plugs derived from mice treated with OMA, the phosphorylation of these signaling components was significantly elevated compared to that in control samples (Fig. 3B). This suggests that activation of the ATM-Chk2-E2F1 signaling axis contributes, at least in part, to the enhancing effect of OMA on pVHL-mediated HIF-1α degradation, and is reflected in the suppression of VEGF expression.

Next, we attempted to elucidate the mechanism through which OMA treatment leads to an elevation of ATM kinase activation in these signaling axes. It has been well established that coordination between cytoplasmic and nuclear activities is vital for cellular homeostasis, and several signaling molecules and transcription factors, such as ATM kinase and the tumor suppressor p53, are regulated by intracellular ROS during this intracellular communication [32,68]. OMA, a tricarboxylic acid (α-hydroxy-β-oxalosuccinic acid) formed in *in vitro* and *in vivo* by condensation of oxaloacetate and glyoxylate (Supplementary Figure 1A), is known to be a potent competitive inhibitor of $NADP^+$-dependent isocitrate dehydrogenase isoform 1 (IDH1) and isoform 2 (IDH2), which are localized to the cytoplasm and mitochondria, respectively [23,24]. In particular, both IDH enzyme isoforms are the primary NADPH producers within their respective subcellular compartments, and thus play a critical role in cellular redox regulation through maintaining the NADPH-dependent GSH/GSSG ratio [37–39]. Therefore, this strongly suggests that inhibition of IDH enzymes by OMA modulates the cellular redox status, and is thus responsible for the regulation of this signaling pathway. As expected, the enzymatic activity of both IDH1 and IDH2 was significantly inhibited by OMA treatment in RPE cells without measureable changes in the overall levels of IDH enzymes (Supplementary Figure 1B and C). We next inhibited IDH activity and examined the effect on the redox status of mitochondria and intracellular ROS production; we analyzed the mitochondrial redox (Fig. 3C), mitochondrial membrane potential (Fig. 3D), and intracellular ROS (Fig. 3E and F) in the absence and presence of OMA. The data revealed that inactivation of IDH enzymes by OMA led to elevated levels of mitochondrial ROS, associated with alteration of mitochondrial membrane potential, and an increase in intracellular ROS levels in RPE cells. This suggests an overall increase in cellular ROS in RPE cells after OMA treatment. Taken together, the data in Fig. 3 indicate that inhibition of IDH enzymes by OMA, resulting in elevated cellular ROS production, regulates the ROS-dependent ATM-mediated E2F1 axis in RPE cells.

Fig. 3G summarizes the mechanistic findings of our study as follows: OMA reduces the activity of IDH enzymes as a competitive inhibitor in RPE cells, resulting in an elevation of intracellular ROS, which leads to the activation of the E2F1 transcription factor. This occurs *via* regulation of the ROS-mediated ATM-Chk2 signaling axis, resulting from the modulation of the cellular redox status. As a result, the activation of E2F1 leads to upregulation of pVHL activity, which in turn inhibits VEGF production by promoting HIF-1α degradation. These data therefore indicate a critical role for OMA in the inhibition of VEGF-mediated angiogenesis.

3.4. Effect of OMA on age-related macular degeneration with choroidal neovascularization

Next, we determined whether inhibition of VEGF expression through OMA in RPE cells could be used for therapeutic purposes. RPE-derived VEGF is considered one of the key molecules for the formation of CNV in AMD [13,14]. Hence, we reasoned that OMA might inhibit CNV-related angiogenesis with a specific focus on suppression of RPE-related VEGF production. We used a polyethylene glycol (PEG)-induced mouse model of AMD [54,55] to test the efficacy of OMA in treating CNV development and retinal dysfunction. The AMD mouse model was established in 8-week-old male C57BL/6 J mice by subretinal injection of PEG-8 [55]. The mice subsequently received 4 μg of OMA by intravitreal injection, immediately following the induction of CNV formation. Following the treatment, we performed a histological investigation of the paraffin sections from mouse eyes. Light microscopic evaluation of the outer retina and choroidal tissues of PEG-8-injected mice revealed distinct organizational changes compared to control tissues (Fig. 4A). The CC, which normally forms a continuous plexus beneath the Bruch's membrane (BrM), was replaced by enlarged and discontinuous vessels. Moreover, the changes in the choroidal vasculature were associated with RPE dysfunction, evidenced by the presence of increased density of RPE cell nuclei.

However, the pathological phenotype of the RPE-BrM-CC complex, the hallmarks of AMD pathology [69], were significantly reduced in these regions upon treatment with OMA (to a level comparable to that seen in controls). In parallel with the effect on the choroidal vasculature, administration of OMA drastically suppressed CNV-related angiogenesis, the hallmark of AMD [4,5], which was localized between the two layers of cytokeratin 18-positive RPE cells in the subretinal place. In contrast, the prominent choroidal vessels were located exclusively within the choroid in the PEG-8-injected mice compared that observed in controls (Fig. 4B). *In vivo* measurement of VEGF expression in the RPE after OMA treatment revealed that there was a massive decrease in VEGF-positive staining in the apical side of the RPE, and within the choroid, compared that in PEG-8-treated mice.

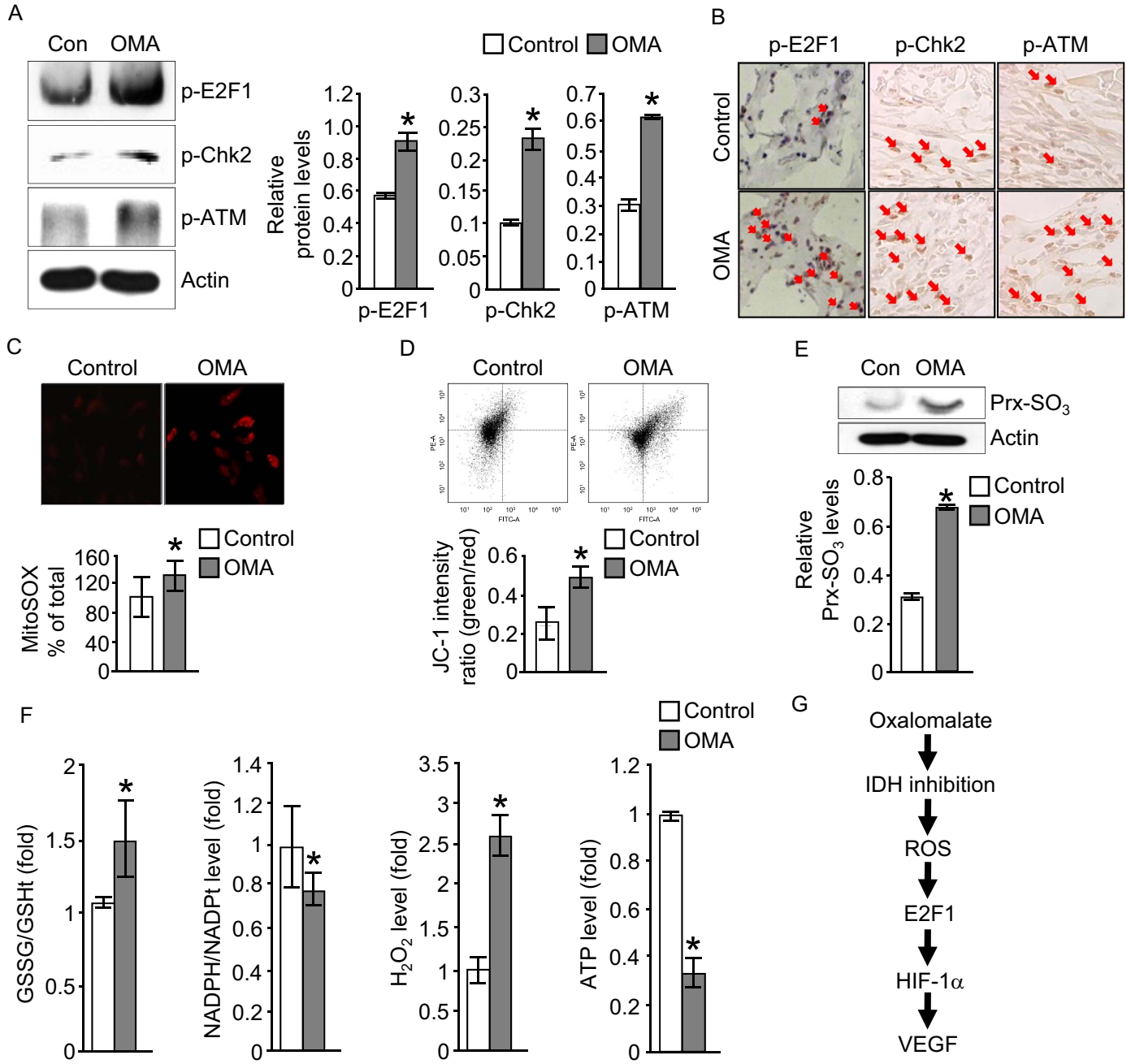

Fig. 3. OMA regulates ROS-dependent E2F1 activation. (A) Immunoblot analysis of proteins related ATM-mediated E2F1 activation from the RPE cells following treatment with OMA (5 mM, 24 h). Actin was used as a loading control. Quantifications of the levels of the indicated proteins are normalized to the expression of actin and shown. (B) Immunohistochemical analysis for proteins involved in ATM signaling axis from Matrigel plugs mixed with the PRE cells in the presence of OMA. Shown are the quantifications of the levels of the indicated proteins as a percentage of control. (C) MitoSOX fluorescence level for evaluation of mitochondrial ROS generation in the RPE cells treated with OMA. Histograms represent the quantification of fluorescence intensity. (D) Flow cytometric analysis of mitochondrial transmembrane potential (MMP) in the RPE cells. The cells were grown in the presence or absence of 5 mM OMA for 24 h, and JC-1, the mitochondrial fluorescent probe, staining followed by FACS analysis was used to assayed MMP. Loss of MMP was demonstrated by the change in the JC-1 fluorescence form red (JC-1 aggregates; mitochondria with high MMP) to green (JC-1 monomers; mitochondria with low MMP). Quantifications of MMP are expressed as a ratio of JC-1 (green/red) in the different treatment groups. (E) Immunoblot analysis of Prx-SO_3 levels in the RPE cells untreated or treated with OMA. Actin was used as a loading control. Quantifications of the protein levels normalized to actin are shown. (F) Ratio of GSSG *versus* total GSH concentration, ratio of NADPH *versus* total NADP concentration, intracellular peroxide production, and ATP levels were measured in the RPE cells following the OMA treatment. Values are presented as the fold change over the levels observed in the control. (G) Model for the regulation of HIF-1α-mediated VEGF expression through ROS-controlled E2F1 activity in the RPE cells and the consequence of inhibition of IDH enzymes by OMA. Data are presented as the mean ± SD of three independent experiments. *$P < 0.01$, *versus* control group. The figure shows representative data for three independent experiments. (For interpretation of the references to color in this figure legend, the reader is referred to the web version of this article.)

This was indicative of a favorable response to OMA treatment in the RPE, which is the main producer of CNV-related VEGF (Fig. 4C). Thus, results obtained from the *in vivo* mouse model of AMD support the prediction based on experiments with cultured cells that OMA inhibits CNV-related angiogenesis by suppressing RPE-mediated VEGF expression.

In conclusion, our findings demonstrate that OMA is able to reduce the expression and secretion of VEGF in RPE cells through the subsequent regulation of multiple mechanisms as follows: (1) modulation of the intracellular ROS through inhibition of IDH enzymes; (2) promotion of the ROS-dependent ATM-Chk2-E2F1 signaling axis; (3) activation of pVHL-mediated HIF-1α degradation. Moreover, in light

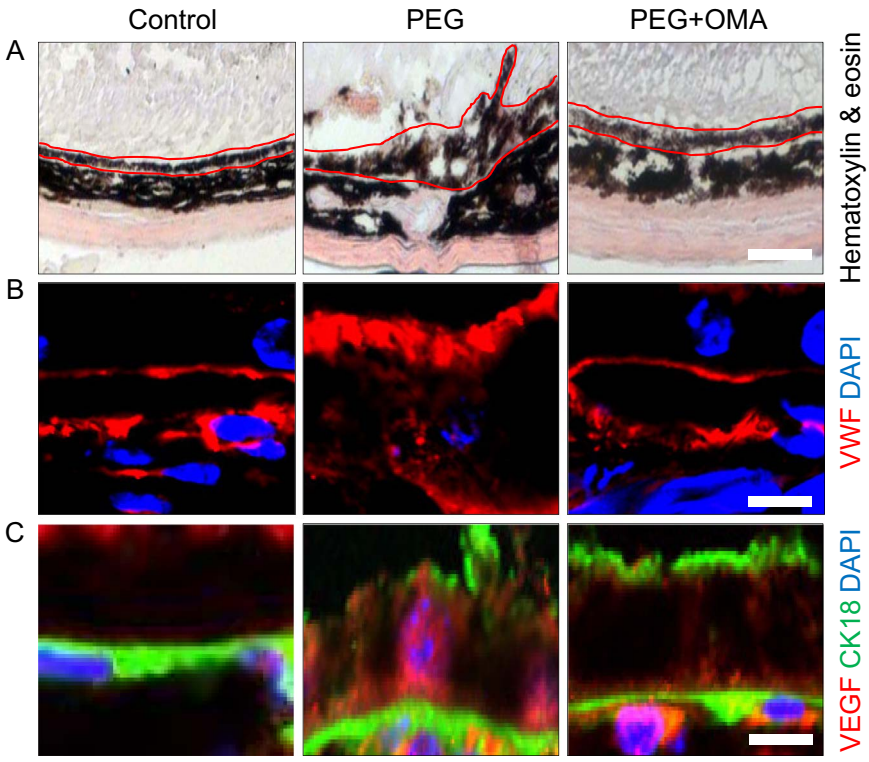

Fig. 4. OMA inhibits RPE-derived VEGF expression and CNV development in the mouse model of AMD. (A) Representative hematoxylin and eosin-stained section of the outer retina and choroidal tissues from mice treated as described in the panel (n =7). (B and C) Immunohistochemical staining for choroidal vasculature (B) and RPE-derived VEGF expression (C) detected with anti-VWF and anti-VEGF antibodies (red color), respectively, in the different treatment groups (n =7). Nuclei were detected with DAPI (blue). Shown are the merged images, associated with RPE cell-specific marker, cytokeratin 18 (CK18, green color). The animals were sacrificed at day 3 post-injection, as outlined in Materials and Methods, and subjected for the histological analyses. The panels on the left represent normal structures of the RPE-choroid after PBS injection. Dotted lines represent layers of the RPE cells in the subretinal space. Bars in the histological sections indicate 10 μm. The figure shows representative data for five independent experiments. (For interpretation of the references to color in this figure legend, the reader is referred to the web version of this article.)

of the essential role for RPE-derived VEGF in CNV formation during AMD, our data strongly support the hypothesis that OMA inhibits CNV formation by reducing RPE-derived VEGF production, and thus suggest the potential development of OMA for therapeutic approaches targeting AMD pathogenesis.

Acknowledgements

We appreciate the help of our laboratory members, in particular Ye Jin Lim and Jeong Ho Kim for critically reading the manuscript and providing useful comments. We are grateful to Suk Hee Lee, Jeong Hoon Pan, Jun Ho Kim, and Young Jun Kim for critical comments and helpful discussions regarding the manuscript. We acknowledge the service of the Biomedical Research Imaging Center at Kyungpook National University, Republic of Korea. This work was supported by the National Research Foundation of Korea, South Korea (NRF) grant funded by the Korean government (MSIP) (NRF-2015R1A4A1042271 and NRF-2015R1C1A1A01053746) and granted by Korea University. No potential conflicts of interest relevant to this article are reported.

Appendix A. Supporting information

Supplementary data associated with this article can be found in the online version at doi:10.1016/j.redox.2016.10.008.

References

[1] D.I. Holmes, I. Zachary, The vascular endothelial growth factor (VEGF) family: angiogenic factors in health and disease, Genome Biol. 6 (2) (2005) 209.
[2] R.B. Bhisitkul, Vascular endothelial growth factor biology: clinical implications for ocular treatments, Br. J. Ophthalmol. 90 (12) (2006) 1542–1547.
[3] N. Ferrara, H.P. Gerber, J. LeCouter, The biology of VEGF and its receptors, Nat. Med. 9 (6) (2003) 669–676.
[4] J. Ambati, B.K. Ambati, S.H. Yoo, S. Ianchulev, A.P. Adamis, Age-related macular degeneration: etiology, pathogenesis, and therapeutic strategies, Surv. Ophthalmol. 48 (3) (2003) 257–293.
[5] M. Lu, A.P. Adamis, Molecular biology of choroidal neovascularization, Ophthalmol. Clin. North Am. 19 (3) (2006) 323–334.
[6] D.W. Miller, A.M. Joussen, F.G. Holz, The molecular mechanisms of neovascular age-related macular degeneration, Ophthalmologe 100 (2) (2003) 92–96.
[7] M. Kliffen, H.S. Sharma, C.M. Mooy, S. Kerkvliet, P.T. de Jong, Increased expression of angiogenic growth factors in age-related maculopathy, Br. J. Ophthalmol. 81 (2) (1997) 154–162.
[8] M. Saint-Geniez, A.E. Maldonado, P.A. D'Amore, VEGF expression and receptor activation in the choroid during development and in the adult, Invest Ophthalmol. Vis. Sci. 47 (7) (2006) 3135–3142.
[9] H.G. Blaauwgeers, G.M. Holtkamp, H. Rutten, A.N. Witmer, P. Koolwijk, T.A. Partanen, K. Alitalo, M.E. Kroon, A. Kijlstra, V.W. van Hinsbergh, R.O. Schlingemann, Polarized vascular endothelial growth factor secretion by human retinal pigment epithelium and localization of vascular endothelial growth factor receptors on the inner choriocapillaris. Evidence for a trophic paracrine relation, Am. J. Pathol. 155 (2) (1999) 421–428.
[10] R. Kannan, N. Zhang, P.G. Sreekumar, C.K. Spee, A. Rodriguez, E. Barron, D.R. Hinton, Stimulation of apical and basolateral VEGF-A and VEGF-C secretion by oxidative stress in polarized retinal pigment epithelial cells, Mol. Vis. 12 (2006) 1649–1659.
[11] H.P. Gerber, A. McMurtrey, J. Kowalski, M. Yan, B.A. Keyt, V. Dixit, N. Ferrara, Vascular endothelial growth factor regulates endothelial cell survival through the phosphatidylinositol 3'-kinase/Akt signal transduction pathway. Requirement for Flk-1/KDR activation, J. Biol. Chem. 273 (46) (1998) 30336–30343.
[12] A.K. Olsson, A. Dimberg, J. Kreuger, L. Claesson-Welsh, VEGF receptor signalling - in control of vascular function, Nat. Rev. Mol. Cell Biol. 7 (5) (2006) 359–371.
[13] P.A. Campochiaro, P. Soloway, S.J. Ryan, J.W. Miller, The pathogenesis of choroidal neovascularization in patients with age-related macular degeneration, Mol. Vis. 5 (1999) 34.
[14] R.O. Schlingemann, Role of growth factors and the wound healing response in age-related macular degeneration, Graefes Arch. Clin. Exp. Ophthalmol. 242 (1) (2004) 91–101.
[15] P.A. D'Amore, Mechanisms of retinal and choroidal neovascularization, Invest. Ophthalmol. Vis. Sci. 35 (12) (1994) 3974–3979.
[16] M.S. Ip I.U. Scott G.C. Brown M.M. Brown A.C. Ho S.S. Huang F.M. Recchia O. American Academy of, Anti-vascular endothelial growth factor pharmacotherapy for age-related macular degeneration: a report by the American Academy of

Ophthalmology Ophthalmology 115 (10) 2008, pp.1837–1846.
[17] T.Y. Wong, G. Liew, P. Mitchell, Clinical update: new treatments for age-related macular degeneration, Lancet 370 (9583) (2007) 204–206.
[18] R.B. Andriolo, M.E. Puga, R. Belfort Junior, A.N. Atallah, Bevacizumab for ocular neovascular diseases: a systematic review, Sao Paulo Med. J. 127 (2) (2009) 84–91.
[19] H. Kourlas, P. Abrams, Ranibizumab for the treatment of neovascular age-related macular degeneration: a review, Clin. Ther. 29 (9) (2007) 1850–1861.
[20] E.W. Ng, D.T. Shima, P. Calias, E.T. Cunningham Jr., D.R. Guyer, A.P. Adamis, Pegaptanib, a targeted anti-VEGF aptamer for ocular vascular disease, Nat. Rev. Drug Disco. 5 (2) (2006) 123–132.
[21] R. Simo, C. Hernandez, Intravitreous anti-VEGF for diabetic retinopathy: hopes and fears for a new therapeutic strategy, Diabetologia 51 (9) (2008) 1574–1580.
[22] M. Slevin, P. Kumar, Q. Wang, S. Kumar, J. Gaffney, M. Grau-Olivares, J. Krupinski, New VEGF antagonists as possible therapeutic agents in vascular disease, Expert Opin. Invest. Drugs 17 (9) (2008) 1301–1314.
[23] O.C. Ingebretsen, Mechanism of the inhibitory effect of glyoxylate plus oxaloacetate and oxalomalate on the NADP-specific isocitrate dehydrogenase, Biochim. Biophys. Acta 452 (2) (1976) 302–309.
[24] A. Ruffo, R. Moratti, A. Montani, G.L. d'Eril, inhibition by oxalomalate of isocitrate (NADP+) dehydrogenase, Ital. J. Biochem. 23 (6) (1974) 357–370.
[25] A. Adinolfi, V. Guarriera-Bobyleva, S. Olezza, A. Ruffo, Inhibition by oxalomalate of rat liver mitochondrial and extramitochondrial aconitate hydratase, Biochem. J. 125 (2) (1971) 557–562.
[26] R.A. Johanson, H.C. Reeves, Concerted inhibition of NADP+-specific isocitrate dehydrogenase by oxalacetate and glyoxylate. I. Oxalomalate formation and stability, and nature of the enzyme inhibition, Biochim. Biophys. Acta 483 (1) (1977) 24–34.
[27] R. Bais, A.M. Rofe, R.A. Conyers, Investigations into the effect of glyoxylate decarboxylation and transamination on oxalate formation in the rat, Nephron 57 (4) (1991) 460–469.
[28] W.L. Davis, J.L. Matthews, D.B. Goodman, Glyoxylate cycle in the rat liver: effect of vitamin D3 treatment, FASEB J. 3 (5) (1989) 1651–1655.
[29] S. Fujiwara, T. Noguchi, Degradation of purines: only ureidoglycollate lyase out of four allantoin-degrading enzymes is present in mammals (Pt 1)Biochem. J. 312 (1995) 315–318.
[30] S.J. Kwon, J.W. Park, W.K. Choi, I.H. Kim, K. Kim, Inhibition of metal-catalyzed oxidation systems by a yeast protector protein in the presence of thioredoxin, Biochem Biophys. Res. Commun. 201 (1) (1994) 8–15.
[31] H. Sies, Biochemistry of oxidative stress, Angew. Chem. Int. Ed. 25 (12) (1986) 1058–1071.
[32] Z. Guo, S. Kozlov, M.F. Lavin, M.D. Person, T.T. Paull, ATM activation by oxidative stress, Science 330 (6003) (2010) 517–521.
[33] K. Iwasaki, E.L. Mackenzie, K. Hailemariam, K. Sakamoto, Y. Tsuji, Hemin-mediated regulation of an antioxidant-responsive element of the human ferritin H gene and role of Ref-1 during erythroid differentiation of K562 cells, Mol. Cell Biol. 26 (7) (2006) 2845–2856.
[34] P.D. Ray, B.W. Huang, Y. Tsuji, Reactive oxygen species (ROS) homeostasis and redox regulation in cellular signaling, Cell Signal. 24 (5) (2012) 981–990.
[35] J.H. Seo, Y. Ahn, S.R. Lee, C. Yeol Yeo, K. Chung Hur, The major target of the endogenously generated reactive oxygen species in response to insulin stimulation is phosphatase and tensin homolog and not phosphoinositide-3 kinase (PI-3 kinase) in the PI-3 kinase/Akt pathway, Mol. Biol. Cell 16 (1) (2005) 348–357.
[36] K. Tobiume, A. Matsuzawa, T. Takahashi, H. Nishitoh, K. Morita, K. Takeda, O. Minowa, K. Miyazono, T. Noda, H. Ichijo, ASK1 is required for sustained activations of JNK/p38 MAP kinases and apoptosis, EMBO Rep. 2 (3) (2001) 222–228.
[37] S.H. Jo, M.K. Son, H.J. Koh, S.M. Lee, I.H. Song, Y.O. Kim, Y.S. Lee, K.S. Jeong, W.B. Kim, J.W. Park, B.J. Song, T.L. Huh, Control of mitochondrial redox balance and cellular defense against oxidative damage by mitochondrial NADP+-dependent isocitrate dehydrogenase, J. Biol. Chem. 276 (19) (2001) 16168–16176.
[38] S.M. Lee, H.J. Koh, D.C. Park, B.J. Song, T.L. Huh, J.W. Park, Cytosolic NADP(+)-dependent isocitrate dehydrogenase status modulates oxidative damage to cells, Free Radic. Biol. Med. 32 (11) (2002) 1185–1196.
[39] D.E. Koshland Jr., K. Walsh, D.C. LaPorte, Sensitivity of metabolic fluxes to covalent control, Curr. Top. Cell Regul. 27 (1985) 13–22.
[40] K. Smolkova, P. Jezek, The Role of Mitochondrial NADPH-Dependent Isocitrate Dehydrogenase in Cancer Cells, Int. J. Cell Biol. 2012 (2012) 273947.
[41] U.J. Jung, O.S. Kwon, Y.B. Park, T.L. Huh, M.K. Lee, M.S. Choi, Effect of oxalomalate on lipid metabolism and antioxidant defense system in rats, J. Biochem. Mol. Toxicol. 17 (5) (2003) 295–302.
[42] I.Y. Choi, J.W. Park, Sensitization of U937 cells to heat shock by oxalomalate, a competitive inhibitor of NADP+-dependent isocitrate dehydrogenase, Free Radic. Res. 37 (10) (2003) 1099–1105.
[43] C. Irace, G. Esposito, C. Maffettone, A. Rossi, M. Festa, T. Iuvone, R. Santamaria, L. Sautebin, R. Carnuccio, A. Colonna, Oxalomalate affects the inducible nitric oxide synthase expression and activity, Life Sci. 80 (14) (2007) 1282–1291.
[44] H.J. Kim, J.W. Park, Oxalomalate, a competitive inhibitor of NADP+-dependent isocitrate dehydrogenase, regulates heat shock-induced apoptosis, Biochem. Biophys. Res. Commun. 337 (2) (2005) 685–691.
[45] E.S. Yang, J.H. Yang, J.E. Park, J.W. Park, Oxalomalate, a competitive inhibitor of NADP+-dependent isocitrate dehydrogenase, regulates lipid peroxidation-mediated apoptosis in U937 cells, Free Radic. Res. 39 (1) (2005) 89–94.
[46] H. Izuta, Y. Chikaraishi, M. Shimazawa, S. Mishima, H. Hara, 10-Hydroxy-2-decenoic acid, a major fatty acid from royal jelly, inhibits VEGF-induced angiogenesis in human umbilical vein endothelial cells, Evid.-Based Complement. Altern. Med.: eCAM 6 (4) (2009) 489–494.
[47] M.H. Pourgholami, L.M. Khachigian, R.G. Fahmy, S. Badar, L. Wang, S.W. Chu, D.L. Morris, Albendazole inhibits endothelial cell migration, tube formation, vasopermeability, VEGF receptor-2 expression and suppresses retinal neovascularization in ROP model of angiogenesis, Biochem. Biophys. Res. Commun. 397 (4) (2010) 729–734.
[48] T.P. Akerboom, H. Sies, Assay of glutathione, glutathione disulfide, and glutathione mixed disulfides in biological samples, Methods Enzymol. 77 (1981) 373–382.
[49] M.E. Anderson, Determination of glutathione and glutathione disulfide in biological samples, Methods Enzymol. 113 (1985) 548–555.
[50] C.R. Zerez, S.J. Lee, K.R. Tanaka, Spectrophotometric determination of oxidized and reduced pyridine nucleotides in erythrocytes using a single extraction procedure, Anal. Biochem. 164 (2) (1987) 367–373.
[51] R.G. Spragg, D.B. Hinshaw, P.A. Hyslop, I.U. Schraufstatter, C.G. Cochrane, Alterations in adenosine triphosphate and energy charge in cultured endothelial and P388D1 cells after oxidant injury, J. Clin. Investig. 76 (4) (1985) 1471–1476.
[52] L. Pellegrini, B. Pucci, L. Villanova, M.L. Marino, G. Marfe, L. Sansone, E. Vernucci, D. Bellizzi, V. Reali, M. Fini, M.A. Russo, M. Tafani, SIRT3 protects from hypoxia and staurosporine-mediated cell death by maintaining mitochondrial membrane potential and intracellular pH, Cell Death Differ. 19 (11) (2012) 1815–1825.
[53] V.V. Lyzogubov, R.G. Tytarenko, P. Jha, J. Liu, N.S. Bora, P.S. Bora, Role of ocular complement factor H in a murine model of choroidal neovascularization, Am. J. Pathol. 177 (4) (2010) 1870–1880.
[54] V.V. Lyzogubov, N.S. Bora, R.G. Tytarenko, P.S. Bora, Polyethylene glycol induced mouse model of retinal degeneration, Exp. Eye Res. 127 (2014) 143–152.
[55] V.V. Lyzogubov, R.G. Tytarenko, J. Liu, N.S. Bora, P.S. Bora, Polyethylene glycol (PEG)-induced mouse model of choroidal neovascularization, J. Biol. Chem. 286 (18) (2011) 16229–16237.
[56] S. Horie, S.J. Robbie, J. Liu, W.K. Wu, R.R. Ali, J.W. Bainbridge, L.B. Nicholson, M. Mochizuki, A.D. Dick, D.A. Copland, CD200R signaling inhibits pro-angiogenic gene expression by macrophages and suppresses choroidal neovascularization, Sci. Rep. 3 (2013) 3072.
[57] G. Neufeld, T. Cohen, S. Gengrinovitch, Z. Poltorak, Vascular endothelial growth factor (VEGF) and its receptors, FASEB J. 13 (1) (1999) 9–22.
[58] H.J. Park, Y. Zhang, S.P. Georgescu, K.L. Johnson, D. Kong, J.B. Galper, Human umbilical vein endothelial cells and Human dermal microvascular endothelial cells offer new insights into the relationship between lipid metabolism and angiogenesis, Stem Cell Rev. 2 (2) (2006) 93–102.
[59] J.W. Lee, S.H. Bae, J.W. Jeong, S.H. Kim, K.W. Kim, Hypoxia-inducible factor (HIF-1)alpha: its protein stability and biological functions, Exp. Mol. Med. 36 (1) (2004) 1–12.
[60] G.L. Semenza, Targeting HIF-1 for cancer therapy, Nat. Rev. Cancer 3 (10) (2003) 721–732.
[61] M. Ivan, W.G. Kaelin Jr., The von Hippel-Lindau tumor suppressor protein, Curr. Opin. Genet Dev. 11 (1) (2001) 27–34.
[62] P.H. Maxwell, M.S. Wiesener, G.W. Chang, S.C. Clifford, E.C. Vaux, M.E. Cockman, C.C. Wykoff, C.W. Pugh, E.R. Maher, P.J. Ratcliffe, The tumour suppressor protein VHL targets hypoxia-inducible factors for oxygen-dependent proteolysis, Nature 399 (6733) (1999) 271–275.
[63] W. Ji, J. Wang, W. Zhang, X. Liu, G. Ouyang, W. Xiao, PVHL acts as a downstream target of E2F1 to suppress E2F1 activity, Biochem. J. 457 (1) (2014) 185–195.
[64] L. Espada, N. Meo-Evoli, P. Sancho, S. Real, I. Fabregat, S. Ambrosio, A. Tauler, ROS production is essential for the apoptotic function of E2F1 in pheochromocytoma and neuroblastoma cell lines, PLoS One 7 (12) (2012) e51544.
[65] N. Raimundo, L. Song, T.E. Shutt, S.E. McKay, J. Cotney, M.X. Guan, T.C. Gilliland, D. Hohuan, J. Santos-Sacchi, G.S. Shadel, Mitochondrial stress engages E2F1 apoptotic signaling to cause deafness, Cell 148 (4) (2012) 716–726.
[66] W.C. Lin, F.T. Lin, J.R. Nevins, Selective induction of E2F1 in response to DNA damage, mediated by ATM-dependent phosphorylation, Genes Dev. 15 (14) (2001) 1833–1844.
[67] C. Stevens, L. Smith, N.B. La Thangue, Chk2 activates E2F-1 in response to DNA damage, Nat. Cell Biol. 5 (5) (2003) 401–409.
[68] B. Liu, Y. Chen, D.K. Clair St, ROS and p53: a versatile partnership, Free Radic. Biol. Med. 44 (8) (2008) 1529–1535.
[69] M. Saint-Geniez, T. Kurihara, E. Sekiyama, A.E. Maldonado, P.A. D'Amore, An essential role for RPE-derived soluble VEGF in the maintenance of the choriocapillaris, Proc. Natl. Acad. Sci. USA 106 (44) (2009) 18751–18756.